Theoretical study of HCl+ : Potential curves, radiative lifetimes, and photodissociation cross sections

Theoretical study of HCl^+: Potential curves, radiative lifetimes, and photodissociation cross sections

Atul D. Pradhan,[a] Kate P. Kirby, and A. Dalgarno
Harvard–Smithsonian Center for Astrophysics, Cambridge, Massachusetts 02139

(Received 21 June 1991; accepted 30 August 1991)

Configuration interaction wave functions and potential energy curves have been calculated for the four lowest states of $^2\Pi$ and $^2\Sigma^+$ symmetry and the lowest state of $^4\Sigma^-$, $^2\Sigma^-$, $^2\Delta$, and $^4\Pi$ symmetry for the molecular ion HCl^+. Dipole moment functions of the $X\,^2\Pi$ and $A\,^2\Sigma^+$ states are presented as well as dipole moments for transitions from the X state to dipole-allowed excited states. The electronic wave functions were constructed to give a balanced description of Rydberg–valence interactions. The computed radiative lifetime of the $X\,^2\Pi(v=1)$ is found to be in good agreement with previous theoretical and experimental values. Oscillator strengths, transition probabilities, and radiative lifetimes are calculated for the $A\,^2\Sigma^+$–$X\,^2\Pi$ transition for vibrational levels $v' \leqslant 6$ and compared to previous theoretical and experimental results. Vibrational levels $v' \geqslant 7$ of the $A\,^2\Sigma^+$ state are predissociated by the $^4\Pi$, $^4\Sigma^-$, and $^2\Sigma^-$ states. Theoretical photodissociation cross sections are calculated showing that photodissociation occurs primarily through absorption into the (3) $^2\Pi$ and (3) $^2\Sigma^+$ states in the wavelength region $\lambda < 100$ nm and also the $^2\Sigma^-$, $^2\Delta$, and (2) $^2\Pi$ states for wavelengths $\lambda > 100$ nm.

I. INTRODUCTION

We report here an extensive study of ten low-lying electronic states of HCl^+ in order to describe accurately the photodissociation of HCl^+ in radiation fields and to characterize the molecular states that control the charge transfer process,

$$H^+ + Cl \rightleftharpoons H + Cl^+ \qquad (1)$$

at thermal energies. The photodissociation of HCl^+ and the charge transfer process (1) are important elements in the chemistry of chlorine compounds in interstellar clouds.[1]

The $A\,^2\Sigma^+$–$X\,^2\Pi$ emission spectrum of the molecular ion HCl^+ and its isotopes has been investigated experimentally by Sheasley and Mathews,[2] Mohlmann, Bhutani and de Heer,[3] Martner *et al.*,[4] Glenewinkel-Meyer *et al.*,[5] and Rodrigues and Campos[6] and empirical values of the transition dipole moment have been obtained.[3,6] The lifetime of the $A\,^2\Sigma^+$ $(v=0)$ vibrational level has been measured by Martner *et al.*[4] and the lifetime of the $v=1$ vibrational level of the ground $X\,^2\Pi$ state has been measured by Heninger *et al.*[7] and Javahery *et al.*[8]

In theoretical studies, Raferty and Richards[9] in a self-consistent field (SCF) calculation have drawn attention to the possible predissociation of the $A\,^2\Sigma^+$ state by spin–orbit coupling with the $^4\Pi$ state. Werner *et al.*[10] have utilized paired natural orbital-configuration interaction (PNO-CI) and multiconfiguration self-consistent field-self-consistent electron pair (MCSCF-SCEP) methods to compute more accurate potential curves for the $X\,^2\Pi$ and $A\,^2\Sigma^+$ states, dipole moments, and lifetimes of the vibrational levels of the $A\,^2\Sigma^+$ and $X\,^2\Pi$ states.

In this paper, we investigate the states of HCl^+ which separate to $H + Cl^+(^3P)$, $H^+ + Cl(^2P^0)$, $H + Cl^+(^1D)$, and $H + Cl^+(^1S)$ and compare our results for the $X\,^2\Pi$ and $A\,^2\Sigma^+$ states, the A–X transition moment functions, the $X\,^2\Pi$ dipole moment function and the radiative lifetimes with previous studies. Photodissociation cross sections have been obtained for transitions from the lowest vibrational level of the ground state, $X\,^2\Pi$ to the repulsive electronic states of $^2\Sigma^+$ $^2\Sigma^-$, $^2\Pi$, and $^2\Delta$ symmetries.

II. COMPUTATIONAL METHOD

Figure (1) shows the seven lowest separated atom limits of HCl^+ with their energy differences. States that are connected to the ground $X\,^2\Pi$ state by dipole transitions have $^2\Pi$, $^2\Sigma^+$, $^2\Sigma^-$, and $^2\Delta$ symmetries. According to the Wigner–Witmer correlation rules, electronic states with $^2\Pi$ symmetry correlate with the lowest three asymptotes and states with $^2\Sigma^+$ symmetry separate to $H^+ + Cl(^2P^0)$, $H + Cl^+(^1D)$, and $H + Cl^+(^1S)$. The $^2\Sigma^-$, $^4\Sigma^-$, and $^4\Pi$ states correlate with the ground state dissociation limits and the $^2\Delta$ symmetry state separates to $H + Cl^+(^1D)$. Many of the excited states are expected to have significant Rydberg–valence mixing at small nuclear separations and we attempt to include a balanced treatment of both valence and Rydberg character of the states in our wave functions.

A fourth state of $^2\Pi$ symmetry and a fourth state of $^2\Sigma^+$ symmetry are included in this study, since they can be populated by electric dipole transitions from the ground state and may play a role in photodissociation. It is expected that these states exhibit a high degree of Rydberg character and considerable configuration mixing with the many states that lie in close proximity. Thus the computational results for these high-lying states are only qualitative, our purpose being to explore their possible significance for photodissociation and not to provide definitive results on their structure.

[a] Also Department of Physics, Massachusetts Institute of Technology, Cambridge, Massachusetts 02139.

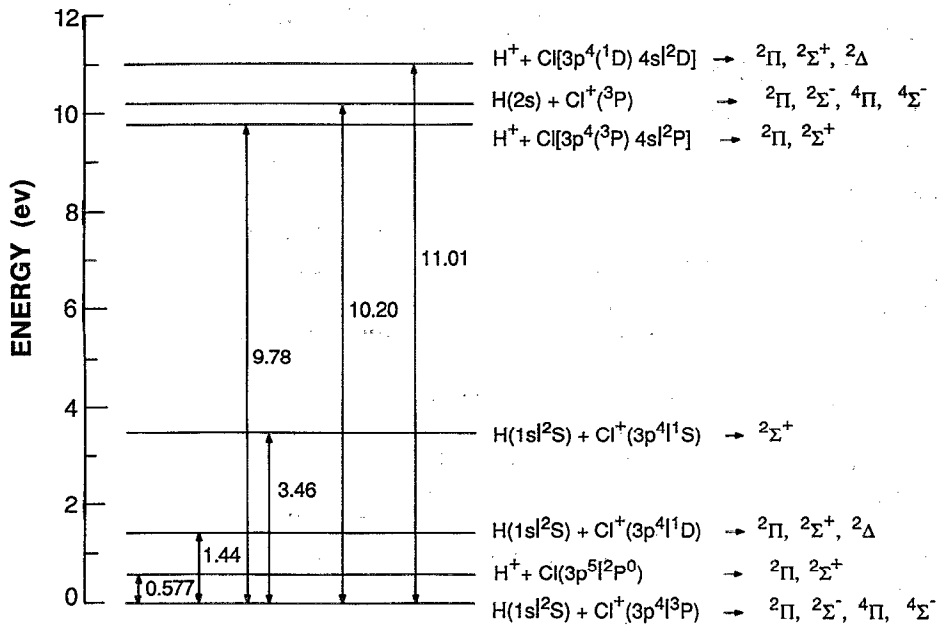

FIG. 1. Separated atom energy splittings.

The electronic energies and wave functions were calculated using the configuration interaction (CI) method. Each wave function was expanded in an orthonormal, n-particle basis set of $C_{\infty v}$ symmetry and equivalence restricted configuration state functions (CSFs). These CSFs were linear combinations of Slater determinants which have the appropriate molecular symmetry and multiplicity. The Slater determinants were constructed from an orthonormal set of molecular orbitals which were expanded in terms of an elementary basis set of Slater-type functions (STF) centered at the atomic nuclei.

The STF basis set used in these calculations is given in Table I. The $(8s/6p/3d/2f)$ chlorine basis set of McLean[11] was augmented by an additional angular correlating $4d$ function. Rydberg $4s$ and $4p$ functions, with exponents of 1.1 and 0.4, respectively, were included in order to construct orbitals (whose description is given below) suitable in accounting for the Rydberg character in the excited states. The hydrogen basis set $(5s/3p/1d)$ was obtained taken from Saxon *et al.*[13]

In the molecular binding region, the $X\,^2\Pi$ state of HCl^+ has as its primary configuration $1\sigma^2 2\sigma^2 3\sigma^2 1\pi^4 4\sigma^2 5\sigma^2 2\pi^3$ which evolves in the separated atom limit to $\cdots 4\sigma^2 5\sigma 6\sigma 2\pi^3$. At small nuclear separations the 5σ and 6σ orbitals are $3p_{Cl} + 1s_H$ and $3p_{Cl} - 1s_H$, respectively, whereas at large nuclear separations they are localized on the Cl and H nuclei, respectively. An SCF calculation of the ground $X\,^2\Pi$ state at an internuclear distance of 2.5 a_0 (very close to the equilibrium separation $R_e = 2.485\ a_0$) yielded a value of -459.5323 a.u.

For each internuclear distance, the molecular orbitals used in the construction of the CI wave functions were obtained in a three step procedure. First, a complete active space SCF (CASSCF) calculation was performed in which the $1-4\sigma, 1\pi$ orbitals were considered frozen core orbitals and the active space consisted of the $5\sigma, 6\sigma$, and 2π orbitals with five electrons distributed among them. The average energy of the first three $^2\Pi$ states was minimized in the multiconfiguration SCF (MCSCF) calculation in order to improve the description of the asymptotes at large nuclear separations.

TABLE I. Slater-type function basis set for HCl^+.

	Exponent (a_0^{-1})	
nl	Cl	H
$1s$	19.432 8	1.7
$1s$	14.328 44	1.0
$1s$		0.5
$2s$	11.441 09	1.0
$2s$	6.939 64	0.5
$2p$	11.136 31	2.0
$2p$	6.046 72	1.0
$2p$		0.5
$3s$	5.30	
$3s$	4.241 41	
$3s$	2.637 53	
$3s$	1.728 65	
$3p$	4.0	
$3p$	3.305 56	
$3p$	1.998 19	
$3p$	1.295	
$3d$	3.306	
$3d$	1.998	
$3d$	1.295	
$4s$	1.1	
$4p$	0.4	
$4d$	1.45	
$4f$	2.57	
$4f$	1.665	

In order to achieve a balanced description of Rydberg and valence character, it was necessary to obtain realistic Rydberg orbitals and to treat them on a par with the occupied valence orbitals. Rydberg orbitals were obtained by performing a five electron single excitation CI (SECI) with four electrons distributed within the $5\sigma 6\sigma 2\pi$ valence space and one electron excited into a restricted virtual space. The Rydberg orbital was obtained from the lowest Rydberg state after a natural orbital analysis. Valence molecular orbitals from a $^4\Pi$ SCF calculation were used as input to ensure that the 6σ valence orbital was an occupied, not a correlating orbital.

For the σ Rydberg orbital the valence space was subdivided into the $5\sigma 6\sigma$ and 2π orbital partitions each of which was doubly occupied. The virtual space consisted of 25 σ orbitals in one partition and all other virtual orbitals in the other partition. The SECI was of $^2\Sigma^+$ symmetry and only single excitations were permitted into the space of 25 σ orbitals. After natural orbital analysis, identification of the lowest σ-type orbital with Rydberg character was made. It was composed primarily of the chlorine $4s$ basis function with coefficient $C(4s) = 0.66$ at a nuclear separation of $R = 1.5\ a_0$. At larger nuclear separations, this orbital progressively displayed more chlorine $3d$ character so that at $R = 2.5\ a_0$ it was composed almost equally of chlorine $3d$ and $4s$ basis functions.

For the π Rydberg orbital, the SECI was of $^4\Pi$ symmetry and the $5\sigma 6\sigma 2\pi$ valence space was kept intact, while the virtual space was partitioned into the 16 π orbitals and all other orbitals. Single excitations were only permitted into the space of 16 π orbitals. The Rydberg orbital of π symmetry selected after natural orbital analysis was composed primarily of the chlorine $4p$ basis function [$C(4p) = 1.48$ at $R = 1.5\ a_0$] with progressively greater chlorine $3d$ character contamination at larger nuclear separations so that at $R = 2.5\ a_0$, it was also composed equally of chlorine $4p$ and $3d$ basis functions.

In forming the final CI wave function the orbital space was partitioned as follows: $1\sigma - 3\sigma 1\pi$ (core); $4\sigma - 6\sigma 2\pi$ (valence); $7\sigma 3\pi$ (Rydberg); the remaining 24σ, 14π, 7δ, 2ϕ (virtual). The K and L shells of chlorine form the core and the seven electron CI wave function was constructed to account for electron correlation as well as valence–Rydberg mixing. As shown in Table II, all single and double excitations from the valence to the virtual space were included as well as all possible arrangements of one electron in the Rydberg space and the rest of the electrons in the virtual space. A particular distribution of the seven electrons in the CI wave function is represented by three integers $(i\ j\ k)$, where i, j, and k denote the number of electrons in the valence, Rydberg, and virtual space, respectively.

It was found that due to the $3d$ character admixture in the Rydberg orbitals at larger nuclear separations, the Rydberg space had significant correlating behavior even though it was a nominally internal set. This is due to the fact that the $3d$ basis functions are normally used to provide in–out and angular correlation for s-type basis functions. Therefore excitations in which the Rydberg space is kept doubly occupied [i.e. (5 2 0) and (4 2 1)] were essential in order to produce a more energetically favorable CI wave function. The excitation (3 2 2) was not included since it contained quadruple excitations from the valence space, resulting in far too many CSFs to be computationally feasible in a calculation of all 12 molecular states of interest in this study.

The inclusion of the (4 1 2) excitation provides correlation of the internal sets with the Rydberg space singly occupied. Because of the number of excited states and different symmetries desired, it was necessary to restrict the number of configurations arising from this occupation. One calculation with the entire (4 1 2) orbital space was performed at $R = 1.8\ a_0$ for each symmetry. It was found that the only Rydberg configurations contained in the CI wave function which had a coefficient greater than 0.05 were $4\sigma^2 5\sigma 2\pi^3 7\sigma$ and $4\sigma^2 5\sigma^2 2\pi^3 3\pi$ for $^2\Pi$ and $^4\Pi$ symmetry and $4\sigma^2 5\sigma^2 2\pi^2 7\sigma$ and $4\sigma^2\ 5\sigma 2\pi^3 3\pi$ for $^2\Sigma^+$, $^2\Sigma^-$, $^4\Sigma^-$, and $^2\Delta$ symmetry. For the (4 1 2) excitation space, only configurations arising from these reference configurations were allowed giving a restricted (4 1 2) orbital space that was computationally manageable. The total numbers of CSFs for each symmetry are given in Table III.

By retaining all significant Rydberg configurations, the more compact wave function arising from the restricted (4 1 2) excitation space (162 205 CSFs for $^2\Pi$ symmetry) described Rydberg behavior almost as well as the much larger wave function arising from the entire (4 1 2) excitation space (with three times as many CSFs). At $R = 2.5$, the energy of the ground state decreased by less than 0.03 eV for the larger wave function vs the restricted wave function. The

TABLE II. Electron distribution among the valence, Rydberg, and virtual orbital spaces in final CI wave function.

Valence	Rydberg	Virtual
7	0	0
6	1	0
6	0	1
5	1	1
5	0	2
5	2	0
4	2	1
4	1	2[a]

[a] Only restricted Rydberg excitations included (see the text).

TABLE III. Number of configuration state functions (CSFs) for each symmetry. Results refer to wave functions incorporating restricted (4 1 2) excitation space only. For $^2\Pi$ symmetry, the number of CSFs for wave function using entire (4 1 2) excitation space is 365 950.

Symmetry	CSFs
$^2\Pi$	162 205
$^4\Pi$	123 794
$^2\Delta$	120 568
$^2\Sigma^+$	89 530
$^2\Sigma^-$	89 258
$^4\Sigma^-$	71 770

energies of the two excited states of $^2\Pi$ and $^2\Sigma^+$ symmetry decreased by no more than 0.06 eV. Therefore the excitation energies (between the X state and the excited states) decreased by less than 0.03 eV for the larger wave function vs the restricted wave function.

In order to demonstrate the significance of the Rydberg orbitals in the excited states, test calculations were performed comparing the ability of the CI wave functions to describe states of $^2\Pi$ and $^2\Sigma^+$ symmetry with and without the Rydberg orbitals. The CI wave function was as described above (i.e., as given by all excitations in Table II). In the first case, Rydberg orbitals were used for the $7\sigma 3\pi$ Rydberg space whereas in the second case, the regular $7\sigma 3\pi$ MCSCF orbitals obtained from the CASSCF calculation (as described above) were substituted. Thus, in the latter case, the Rydberg character was not removed from the basis set altogether, but appeared only in the virtual space. Table IV shows vertical excitation energies from the lowest states of each symmetry at $R = 2.0\ a_0$. The excitation energies show that significant energy lowering is achieved for the second and third excited states only in the first case, namely when the Rydberg orbitals are included in the internal space. Similar calculations at $R = 2.5\ a_0$ showed that Rydberg behavior is present in the higher lying states even at nuclear separations in the proximity of the potential well minimum of the X state.

No states exhibited Rydberg behavior beyond $R = 3.1\ a_0$ except for the (4) $^2\Pi$ and (4) $^2\Sigma^+$ states, whose long range behavior is not well characterized. Nevertheless, Rydberg orbitals were retained in the CI wave function up to $R = 5.0\ a_0$ to ensure continuity of the potential curves. Beyond $R = 5.0\ a_0$ it was not possible to determine orbitals with significant Rydberg character. The change in energy due to removing the Rydberg orbitals and replacing them with the regular 7σ and 3π MCSCF orbitals at this switchover point was less than 1.2 mhartree in all cases.

Initially only orbitals of σ, π, and δ symmetry were included in the virtual space. At large separations the energies of states separating to the common limit of $H + Cl^+$ should be degenerate, yet the energy differences for states of principal configurations differing by $\lambda = 1$ were significant. For the $^2\Sigma^-$ (principal configuration $\cdots 4\sigma^2 5\sigma^2 6\sigma 2\pi^2$) and $X\,^2\Pi$ (principal configuration $\cdots 4\sigma^2 5\sigma^2 2\pi^3$) states, this energy difference amounted to 0.0247 eV at $R = 20.0\ a_0$. This discrepancy may be attributed to the inclusion of only the δ orbitals which provide an asymmetric degree of correlation for valence configurations differing in the occupation of a single σ and π orbital. Inclusion of the ϕ orbitals eliminated this discrepancy.

All calculations mentioned above were performed using the ALCHEMY system of programs developed by Bagus, Liu, McLean, and Yoshimine, and the ALCHEMY II system of programs developed by Yoshimine, Lengsfield and Liu.

III. RESULTS AND DISCUSSION

A. Potential energy curves

In Tables V and VI we present the energies at 31 internuclear distances for the first three states of $^2\Pi$ and $^2\Sigma^+$ symmetry and the lowest lying of each of the states of $^2\Sigma^-$, $^4\Sigma^-$, $^4\Pi$, and $^2\Delta$ symmetry. Potential curves of all the states are given in Figs. 2 and 3. The calculations for the fourth states of $^2\Pi$ and $^2\Sigma^+$ symmetry are less accurate than the lower lying roots and are given only qualitatively in Figs. 2 and 3.

The calculated and spectroscopic energies of the asymptotic separated atom limits are given in Table VII. For limits involving the ^1S, ^1D, and ^3P terms of Cl^+, the calculated splittings are in excellent agreement with the spectroscopic values. However, the calculated splitting between the $H^+ + Cl(3p^5|^2P^0)$ and $H + Cl^+(3p^4|^3P)$ limits is in error by 0.41 eV. The energy difference between the two limits corresponds to the difference between the ionization potential of hydrogen and that of chlorine. No correlation error is

TABLE IV. Comparison of vertical excitation energies (ΔE) at $R = 2.0\ a_0$ from the $X\,^2\Pi$ state with Rydberg vs MCSCF orbitals employed in $7\sigma 3\pi$ orbital space.

	$^2\Pi$ Symmetry			
	Rydberg		MCSCF	
State	Energy (a.u.) below −459.0 a.u.	ΔE (eV) from X state	Energy (a.u.) below −459.0 a.u.	ΔE (eV) from X state
$X\,^2\Pi$	−0.825 54	...	−0.823 09	...
(2) $^2\Pi$	−0.298 05	14.4	−0.245 83	14.7
(3) $^2\Pi$	−0.250 03	14.7	−0.232 98	15.1
(4) $^2\Pi$	−0.226 96	16.3	−0.201 44	16.9
	$^2\Sigma^+$ Symmetry			
	Rydberg		MCSCF	
State	Energy (a.u.) below −459.0 a.u.	ΔE (eV) from X state	Energy (a.u.) below −459.0 a.u.	ΔE (eV) from X state
$A\,^2\Sigma^+$	−0.654 10	4.67	−0.646 91	4.72
(2) $^2\Sigma^+$	−0.361 61	12.6	−0.350 90	12.8
(3) $^2\Sigma^+$	−0.268 95	15.1	−0.251 97	15.5
(4) $^2\Sigma^+$	−0.231 39	16.2	−0.217 76	16.4

TABLE V. Calculated energies (a.u.) for states of $^2\Pi$ and $^2\Sigma^+$ symmetry relative to -458.0 a.u.

$R(a_0)$	$X\,^2\Pi$	$(2)\,^2\Pi$	$(3)\,^2\Pi$	$A\,^2\Sigma^+$	$(2)\,^2\Sigma^+$	$(3)\,^2\Sigma^+$
1.50	−1.466 23	−0.926 23	−0.852 05	−1.277 68	−0.948 65	−0.863 26
1.60	−1.588 53	−1.051 58	−0.979 67	−1.402 00	−1.078 79	−0.988 53
1.70	−1.678 48	−1.143 63	−1.074 92	−1.494 69	−1.177 97	−1.083 08
1.80	−1.744 31	−1.211 49	−1.147 49	−1.564 01	−1.255 10	−1.161 42
1.90	−1.791 87	−1.261 50	−1.203 86	−1.615 71	−1.314 98	−1.221 96
2.00	−1.825 54	−1.298 05	−1.250 03	−1.654 10	−1.361 61	−1.268 95
2.10	−1.848 66	−1.324 87	−1.291 84	−1.682 42	−1.398 19	−1.305 51
2.20	−1.863 77	−1.347 08	−1.328 38	−1.703 12	−1.427 17	−1.333 91
2.30	−1.872 82	−1.376 10	−1.349 18	−1.718 05	−1.450 48	−1.355 79
2.40	−1.877 28	−1.408 37	−1.359 61	−1.728 60	−1.469 62	−1.372 44
2.50	−1.878 31	−1.438 50	−1.368 86	−1.735 83	−1.485 70	−1.384 83
2.60	−1.876 77	−1.465 86	−1.381 79	−1.740 52	−1.499 52	−1.393 84
2.70	−1.873 35	−1.490 51	−1.396 43	−1.743 29	−1.511 65	−1.400 34
2.90	−1.862 81	−1.532 25	−1.425 39	−1.744 73	−1.532 17	−1.410 15
3.10	−1.849 56	−1.565 17	−1.453 10	−1.742 64	−1.548 95	−1.426 76
3.30	−1.835 32	−1.590 77	−1.479 58	−1.738 50	−1.562 87	−1.453 24
3.50	−1.821 10	−1.610 47	−1.504 60	−1.733 22	−1.574 53	−1.479 65
3.75	−1.804 17	−1.628 66	−1.533 18	−1.725 87	−1.586 65	−1.507 52
4.00	−1.788 66	−1.641 49	−1.558 19	−1.718 33	−1.596 81	−1.529 18
4.50	−1.762 50	−1.656 68	−1.596 97	−1.704 13	−1.613 55	−1.556 66
5.00	−1.742 73	−1.664 10	−1.622 53	−1.692 27	−1.626 87	−1.569 76
5.50	−1.728 58	−1.668 13	−1.637 96	−1.683 17	−1.636 79	−1.575 42
6.00	−1.719 06	−1.670 72	−1.646 16	−1.676 64	−1.643 57	−1.577 65
7.00	−1.709 82	−1.672 85	−1.651 40	−1.669 76	−1.650 19	−1.578 50
8.00	−1.707 14	−1.672 22	−1.652 00	−1.667 90	−1.651 75	−1.578 23
9.00	−1.706 40	−1.671 06	−1.651 88	−1.667 70	−1.651 83	−1.577 95
10.00	−1.706 15	−1.670 44	−1.651 74	−1.668 19	−1.651 73	−1.577 80
12.50	−1.705 99	−1.669 70	−1.651 59	−1.668 56	−1.651 59	−1.577 66
15.00	−1.705 94	−1.669 44	−1.651 54	−1.668 76	−1.651 54	−1.577 61
17.50	−1.705 92	−1.669 31	−1.651 52	−1.668 88	−1.651 52	−1.577 59
20.00	−1.705 91	−1.669 23	−1.651 51	−1.668 94	−1.651 51	−1.577 58

made in describing the hydrogen atom because it has only one electron. Significant correlation error is made in describing $Cl(3p^5)$ as opposed to $Cl^+(3p^4)$ and this may be encountered at different levels in the calculation. The STF basis set may not be sufficient to describe Cl and Cl^+ equivalently, and the Cl $3p\pi$ valence orbital may have slightly different character depending on π^3 vs π^2 occupation. Most significantly, the level of correlation in the wave function (single and double excitations only) simply is not adequate to describe the $Cl(3p^5)$ vs $Cl^+(3p^4)$.

The long range behavior of all the states dissociating to $H + Cl^+$ asymptotes is attractive, due to charge induced dipole effects. All of the repulsive states [except the $(2)\,^2\Sigma^+$] display a minimum between 6.0 and 8.0 a_0 with well depths ranging from approximately 200 to 800 cm^{-1}. Some of this apparent attraction is due to polarization and some is due to basis set superposition error. In a configuration interaction treatment using the counterpoise technique we computed the basis set superposition error in this region to range from 92 cm^{-1} at $R = 6.0\,a_0$ to 24 cm^{-1} at $R = 8.0\,a_0$.

In the $H^+ + Cl(3p^5|^2P^0)$ limit, the principal configurations for the $A\,^2\Sigma^+$ and $(2)\,^2\Pi$ states are $\cdots 5\sigma 2\pi^4$ and $\cdots 5\sigma^2 2\pi^3$, respectively, so that this is a case in which the one unpaired electron produces two distinct configurations differing by one unit of angular momentum along the nuclear axis. The long range ion–atom potential applicable to this case consists of quadrupole and charge induced dipole components given in atomic units by

$$V_m = \frac{Q_m}{2R^3} - \frac{\alpha_m}{2R^4}, \tag{2}$$

where $m = M_L$ is the magnetic quantum number of the neutral atom state, $m = 0$ corresponding to a Σ state and $m = \pm 1$ to the Π state, and α_m is the polarizability of the Cl atom and Q_m its quadrupole moment,

$$Q_m = (-1)^m(2 - |m|)\tfrac{2}{5}\langle r_{3p}^2\rangle. \tag{3}$$

The difference in the long range potentials for the Σ and Π states is

$$V_\Sigma - V_\Pi = \frac{Q_A}{2R^3} - \frac{(\alpha_\Sigma - \alpha_\Pi)}{2R^4}, \tag{4}$$

where the quadrupole anisotropy is

$$Q_A = \tfrac{6}{5}\langle r_{3p}^2\rangle.$$

Reinsch and Meyer[14] using PNO-CEPA configuration expansions obtained the result $\alpha_\Sigma - \alpha_\Pi = 2.16$ for the polarizability anisotropy of chlorine. Using it and fitting our results between $R = 10.0\,a_0$ and $R = 20.0\,a_0$, we obtain a value of $Q_A = 4.76 \pm 0.4$ a.u., in good agreement with the value of $Q_A = 4.87$ a.u. evaluated with the result $\langle r_{3p}^2\rangle = 4.06\,a_0^2$ of Fischer.[15]

TABLE VI. Calculated energies (a.u.) for states of $^2\Sigma^-$, $^2\Delta$, $^4\Sigma^-$, and $^4\Pi$ symmetries relative to -458.0 a.u.

$R(a_0)$	$^2\Sigma^-$	$^2\Delta$	$^4\Sigma^-$	$^4\Pi$
1.50	−0.992 38	−0.976 74	−1.046 24	−0.958 11
1.60	−1.117 29	−1.103 00	−1.172 76	−1.083 37
1.70	−1.210 17	−1.195 03	−1.265 03	−1.175 52
1.80	−1.285 30	−1.268 17	−1.338 09	−1.243 77
1.90	−1.345 65	−1.326 66	−1.396 43	−1.294 81
2.00	−1.394 44	−1.373 71	−1.443 23	−1.334 47
2.10	−1.434 48	−1.412 09	−1.481 24	−1.370 18
2.20	−1.467 90	−1.443 82	−1.512 49	−1.405 72
2.30	−1.496 29	−1.470 45	−1.538 52	−1.439 19
2.40	−1.520 79	−1.493 10	−1.560 46	−1.469 78
2.50	−1.542 19	−1.512 57	−1.579 13	−1.497 53
2.60	−1.561 06	−1.529 47	−1.595 18	−1.522 61
2.70	−1.577 81	−1.544 25	−1.609 07	−1.545 20
2.90	−1.606 08	−1.568 72	−1.631 74	−1.583 55
3.10	−1.628 63	−1.587 88	−1.649 23	−1.613 90
3.30	−1.646 62	−1.602 97	−1.662 86	−1.637 56
3.50	−1.660 89	−1.614 87	−1.673 55	−1.655 78
3.75	−1.674 53	−1.626 21	−1.683 69	−1.672 57
4.00	−1.684 52	−1.634 48	−1.691 09	−1.684 35
4.50	−1.696 82	−1.644 61	−1.700 15	−1.698 01
5.00	−1.702 85	−1.649 49	−1.704 50	−1.704 12
5.50	−1.705 57	−1.651 62	−1.706 38	−1.706 57
6.00	−1.706 62	−1.652 38	−1.707 00	−1.707 32
7.00	−1.706 84	−1.652 39	−1.706 92	−1.707 15
8.00	−1.706 50	−1.652 02	−1.706 52	−1.706 64
9.00	−1.706 24	−1.651 76	−1.706 25	−1.706 31
10.00	−1.706 10	−1.651 62	−1.706 10	−1.706 14
12.50	−1.705 97	−1.651 49	−1.705 97	−1.705 99
15.00	−1.705 93	−1.651 45	−1.705 93	−1.705 94
17.50	−1.705 92	−1.651 44	−1.705 92	−1.705 92
20.00	−1.705 91	−1.651 43	−1.705 91	−1.705 91

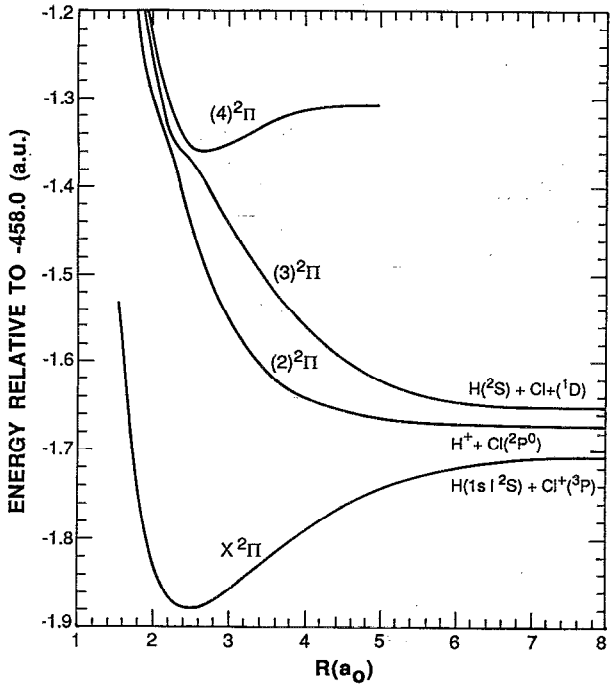

FIG. 2. Potential energy curves of $^2\Pi$ symmetry.

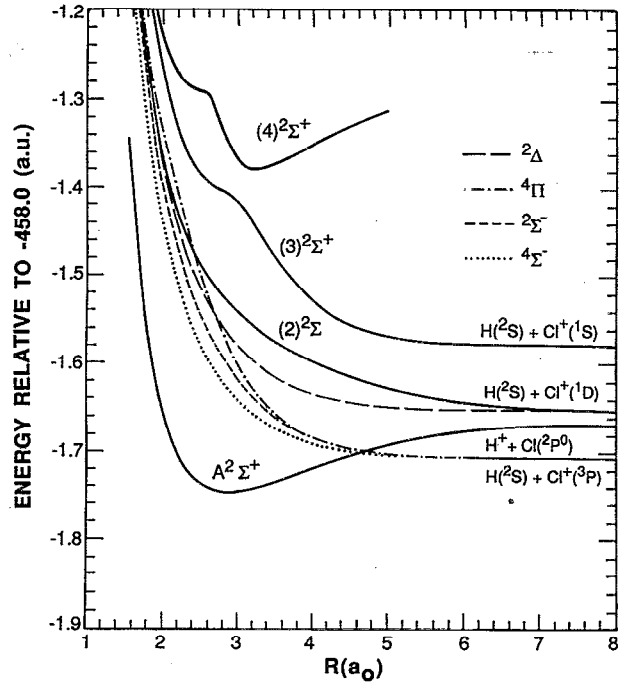

FIG. 3. Potential energy curves of $^2\Sigma^-$, $^2\Delta$, $^4\Sigma^-$, $^4\Pi$, and $^2\Sigma^+$ symmetry.

The $X\,^2\Pi$ and $A\,^2\Sigma^+$ states exhibit Rydberg character only at small internuclear distances, whereas the higher roots of $^2\Pi$ and $^2\Sigma^+$ symmetry show a high degree of valence–Rydberg mixing for $R < 4.5\ a_0$. The $X\,^2\Pi$ state wave function changes smoothly from a $\cdots 5\sigma^2 2\pi^3$ configuration to $\cdots 5\sigma 6\sigma 2\pi^3$ at large R. The $A\,^2\Sigma^+$ state wave function is predominantly composed of the $\cdots 5\sigma 2\pi^4$ configuration at all nuclear separations but also displays some configuration mixing with the (2) $^2\Sigma^+$ state at nuclear separations beyond R_e of the A state involving the $\cdots 6\sigma 2\pi^4$ and $\cdots 5\sigma^2 6\sigma 2\pi^2$ configurations. For $R < 2.5\ a_0$, the avoided crossings of the (2) $^2\Pi$, (3) $^2\Pi$, and (4) $^2\Pi$ states (see Fig. 2) are due to configurational mixing of Rydberg ($\cdots 5\sigma 7\sigma 2\pi^2$ and $\cdots 5\sigma^2 2\pi^2 3\pi$) and valence configurations ($\cdots 5\sigma^2 2\pi^3$ and $\cdots 5\sigma 6\sigma 2\pi^3$). For $R < 2.0\ a_0$, the Rydberg configurations dominate the description of these states. For the (1) $^4\Pi$, (1) $^2\Sigma^-$, (1) $^2\Delta$, and (1) $^4\Sigma^-$ states at small nuclear separations ($R < 2.0\ a_0$) there is minimal interaction with configurations involving the 7σ and 3π Rydberg orbitals while for $R > 2.0\ a_0$ it is not significant. For $R > 2.0\ a_0$ the $^4\Pi$ state is dominated by the $\cdots 5\sigma 6\sigma 2\pi^3$ configuration at all nuclear

TABLE VII. Asymptotic energy splittings (eV) of separated atom limits relative to $H + Cl^+(3p^4|^3P)$.

	Calculated	Spectroscopic
$H^+ + Cl(3p^5|^2P^0)$	0.990	0.581[a]
$H + Cl^+(3p^4|^1S)$	1.48	1.44
$H + Cl^+(3p^4|^1D)$	3.49	3.46

[a] Indicates correlation error in describing Cl wave function is 0.409 eV.

separations while the $^2\Sigma^-$, $^2\Delta$, and $^4\Sigma^-$ states are similarly dominated by the $\cdots 5\sigma^2 6\sigma^2 2\pi^2$ configuration.

Vibrational and rotational energy levels were computed for the bound states by numerical integration of the radial Schrodinger equation,

$$-\frac{\hbar^2}{2\mu}\frac{d^2}{dR^2}\chi_v(R) + \left\{V(R) + \frac{[J(J+1)-\Omega^2]}{2\mu R^2} - E_v\right\}\chi_v(R) = 0, \tag{5}$$

where $V(R)$ is the potential energy and μ the reduced mass. The reduced mass of HCl^+ is 0.979 89 and that of DCl^+ 1.959 78 amu. In determining the rovibrational constants, the same vibrational levels were used as in the study of Sheasley and Mathews. The rovibrational energy levels for $v'' = 0$, 1, and 2 were fitted in the case of the X state to an expression appropriate to Hund's case (a) coupling including only the diagonal portion of the rotational Hamiltonian,

$$T(v,J) = \omega_e(v+\tfrac{1}{2}) - \omega_e x_e(v+\tfrac{1}{2})^2 + B_v[J(J+1)-\Omega^2], \tag{6}$$

where

$$B_v = B_e - \alpha_e(v+\tfrac{1}{2}).$$

Since the A state is of $^2\Sigma^+$ symmetry and belongs to Hund's case (b), the rotational term was taken to be $B_v[N(N+1)-\Lambda^2]$ with $J = N \pm 1/2$ (i.e., rotational levels for the same value of N but different values of J are degenerate). For the $A\,^2\Sigma^+$ state we fitted the $v' = 0$–6 and $v' = 0$–9 levels for HCl^+ and DCl^+, respectively. For the lowest three vibrational bands of both the X and the A state, eight rotational energy levels were used in the fitting procedure while for the higher bands four rotational levels were used. The spectroscopic constants for the X and A states are presented in Table VIII and are compared with the values derived from the experimental data of Sheasley and Mathews,[2] Hotop *et al.*,[16] and Natalis *et al.*[17] For the X state, the agreement between the calculated and experimental rovibrational constants is excellent. The vibrational parameter ω_e of the $A\,^2\Sigma^+$ state is in good agreement with experiment but the anharmonicity parameter $\omega_e x_e$ shows a significant discrepancy. This is most certainly due to the fact that the correlation error in the chlorine ionization potential displaced the $H^+ + Cl(^2P^0)$ asympotote upwards by 0.41 eV thus forcing the calculated $A\,^2\Sigma^+$ state potential curve to rise more steeply between R_e and the separated atom limit. This made the A state potential curve more harmonic thereby reducing $\omega_e x_e$ at intermediate nuclear separations and adversely affecting the position of the higher rovibrational levels. This was demonstrated by repeating the rovibrational analysis for the A state of HCl^+ with the levels of the upper two vibrational bands $v = 5$ and 6 excluded. The resulting values for ω_e and $\omega_e x_e$ were 1593 and 37.2 cm^{-1}, respectively, in much better agreement with experimental values. These improved results attest to the significance of the corre-

TABLE VIII. Spectroscopic constants for the $X\,^2\Pi$ and $A\,^2\Sigma^+$ states.

	R_e (a_0)		D_e (eV)		T_e (eV)
	$X\,^2\Pi$	$A\,^2\Sigma^+$	$X\,^2\Pi$	$A\,^2\Sigma^+$	$X\,^2\Pi$–$A\,^2\Sigma^+$
This work	2.485	2.865	4.69	2.07[e]	3.634
Werner *et al.*[a]	2.493	2.862	···	···	3.573
SM[b] (expt.)	2.485	2.861	···	···	3.549
Hotop[c] *et al.* (expt.)	···	···	4.812(5)[f]	1.856(5)	3.536(10)
NPLC[d] (expt.)	···	···	4.50	2.04	3.452(5)

		$X\,^2\Pi$ (cm^{-1})			
		ω_e	$\omega_e x_e$	α_e	B_e
HCl^+	This work	2672	52.5	0.289	9.82
	Werner *et al.*	2579	···	···	···
	SM	2673	52.0	0.31	9.94
DCl^+	This work	1927	27.5	0.107	5.08
	SM	1918	27.0	0.110	5.11

		$A\,^2\Sigma^+$ (cm^{-1})			
		ω_e	$\omega_e x_e$	α_e	B_e
HCl^+	This work	1572	30.1	0.290	7.40
	Werner *et al.*	1572	···	···	···
	SM	1606	40.3	0.330	7.51
DCl^+	This work	1147	17.7	0.103	3.81
	SM	1152	20.4	0.122	3.85

[a] Sheasley and Mathews. Reference 2.
[b] Werner *et al.* Reference 10.
[c] Hotop *et al.* Reference 16.
[d] Natalis *et al.* Reference 17.
[e] Includes 0.41 eV correlation error in Cl wave function.
[f] Parentheses indicate stated errors.

lation error present in the A state at larger nuclear separations which affects especially the higher vibrational levels.

The correlation error at the separated atom limit contributes to our overestimate of 2.07 eV for the dissociation energy (D_e) of the A state as compared to the value of 1.86 eV given by Hotop *et al.*[16] (Table VIII). Our result of 4.69 eV for the dissociation energy of the $X\,^2\Pi$ state is in good agreement with the experimental value of 4.81 eV.[16] The experimental values of D_e of Natalis *et al.*[17] for the $X\,^2\Pi$ and $A\,^2\Sigma^+$ states are Birge–Sponer extrapolations of vibrational levels accessed in their Penning ionization study and are less reliable than those of Hotop *et al.*[16]

B. Transition moments

The transition dipole moment $D(R)$ between two electronic states is the matrix element over all electronic coordinates of the dipole operator $\mathbf{d} = -\Sigma_i e\,\mathbf{r}_i$ between the initial and final electronic states. Here $\mathbf{r}_i = (x_i, y_i, z_i)$ is the position vector of the ith electron with the z axis along the line joining the nuclei, e is the electronic charge, and the summation is over all electrons. For each fixed R, the transition dipole moment $D(R)$ in atomic units for Σ–Π and Δ–Π transitions is given by the matrix element $\langle\psi_\Sigma| -\Sigma_j(x_j + iy_j)/\sqrt{2}|\psi_\Pi\rangle$ and $\langle\psi_\Delta| -\Sigma_j(x_j + iy_j)/\sqrt{2}|\psi_\Pi\rangle$ respectively. For Π–Π transitions, $D(R)$ reduces to the matrix element of the dipole operator $-\Sigma_j z_j$.

Transition moments between the $X\,^2\Pi$ state and all states which can be accessed by a dipole transition were calculated and are listed in Table IX and shown in Figs. 4 and 5. By performing natural orbital iterations (two cycles) independently upon the $X\,^2\Pi$ and $A\,^2\Sigma^+$ states at $R = 2.5\ a_0$, and then using the output wave functions to compute the A–X transition moment, we found the dipole moment for the A–X transition decreased by 0.011 a.u. or roughly 8%.

The dipole moment for the A–X transition is shown in Fig. 6 and compared to the theoretical results of Werner *et al.*[10] and the analytic form stated by Glenewinkel-Meyer *et al.*,[5] which was derived from their experimental results and normalized to the value of 0.54 D at $R = 1.0$ Å. Our calculated dipole moment compared to the result of Werner *et al.*[10] within the Franck–Condon region for A–X vibrational transitions ($2.4 < R < 3.5\ a_0$) is larger by 0.01 ea_0 at $R = 2.5\ a_0$ and as much as 0.016 ea_0 at $R = 3.0\ a_0$.

The $^2\Sigma^-$ and $^2\Delta$ states are composed of the same principal configurations, but different angular momentum couplings so that their transition moments with the $X\,^2\Pi$ state are very similar in form, as shown in Fig. 4.

The higher states of $^2\Pi$ and $^2\Sigma^+$ symmetry are dominated by Rydberg behavior at small nuclear separations ($R < 2.1\ a_0$) and continue to show significant Rydberg behavior at larger separations where valence configurations dominate their wave functions. The change in sign and magnitude of the transition moment functions depends on the

TABLE IX. Transition moments (a.u.) between the $X\,^2\Pi$ state and dipole accessible states.

$R(a_0)$	$(2)\,^2\Pi$	$(3)\,^2\Pi$	$A\,^2\Sigma^+$	$(2)\,^2\Sigma^+$	$(3)\,^2\Sigma^+$	$^2\Sigma^-$	$^2\Delta$
1.50	0.107	−0.556	0.2556	−0.258	0.000	0.804	0.795
1.60	0.110	−0.526	0.2455	−0.205	0.000	0.744	0.742
1.70	0.113	−0.465	0.2309	−0.141	0.000	0.563	0.595
1.80	0.113	−0.373	0.2192	−0.095	0.019	0.472	0.508
1.90	0.113	−0.251	0.2073	−0.056	0.039	0.407	0.436
2.00	0.111	−0.100	0.1948	−0.023	0.059	0.357	0.374
2.10	0.108	0.016	0.1820	0.003	0.078	0.317	0.321
2.20	0.112	0.038	0.1618	0.024	0.096	0.282	0.277
2.30	0.116	0.033	0.1564	0.038	0.112	0.251	0.238
2.40	0.116	0.147	0.1438	0.048	0.128	0.222	0.205
2.50	0.119	0.461	0.1316	0.054	0.142	0.195	0.177
2.60	0.124	0.778	0.1296	0.057	0.154	0.170	0.152
2.70	0.132	0.967	0.1080	0.057	0.162	0.146	0.130
2.90	0.155	1.210	0.0860	0.054	0.161	0.105	0.096
3.10	0.187	1.373	0.0662	0.048	0.105	0.073	0.069
3.30	0.228	1.491	0.0489	0.042	0.047	0.047	0.048
3.50	0.280	1.583	0.0340	0.034	0.016	0.028	0.033
3.75	0.363	1.675	0.0183	0.024	−0.007	0.009	0.020
4.00	0.468	1.752	0.0051	0.013	−0.021	−0.006	0.011
4.50	0.757	1.866	−0.0159	−0.010	−0.033	−0.025	0.002
5.00	1.164	1.876	−0.0306	−0.029	−0.031	−0.034	−0.001
5.50	1.635	1.685	−0.0389	−0.038	−0.024	−0.034	0.000
6.00	1.975	1.274	−0.0422	−0.038	−0.016	−0.029	0.002
7.00	1.716	0.445	−0.0400	−0.025	−0.005	−0.015	0.005
8.00	0.968	0.107	−0.0313	−0.012	−0.001	−0.006	0.005
9.00	0.462	0.022	−0.0065	−0.001	−0.001	−0.003	0.000
10.00	0.214	0.004	−0.0049	−0.001	−0.001	−0.003	0.000
12.50	0.029	0.000	−0.0024	−0.001	−0.001	−0.002	0.000
15.00	0.004	0.000	−0.0012	−0.001	−0.001	−0.002	0.000
17.50	0.001	0.000	−0.0001	−0.001	0.000	−0.001	0.000
20.00	0.000	0.000	0.0000	0.000	0.000	−0.001	0.000

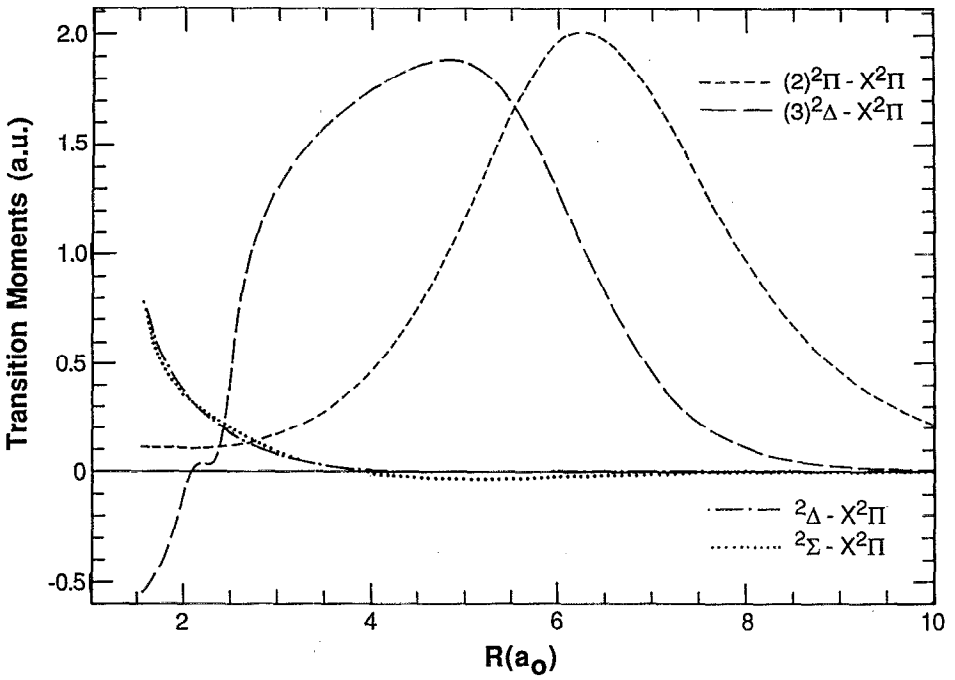

FIG. 4. Transition dipole moments between X state and states of $^2\Pi$, $^2\Sigma^-$, and $^2\Delta$ symmetry.

relative amounts of Rydberg and valence configurations within the final state wave function. The (3) $^2\Pi$ transition moment changes sign as the final state wave function goes from predominantly Rydberg configurations at $R = 2.0\ a_0$ to valence configurations within the Franck–Condon region of the $X\,^2\Pi$ state. The magnitude of the transition moment is greatest when valence configurations predominate. For the (3) $^2\Pi$ state, there is also evident a rapid changeover from the $\cdots 5\sigma^2 2\pi^2 3\pi$ Rydberg configuration to the $\cdots 5\sigma 6\sigma 2\pi^3$ configuration within the valence region causing sudden decrease of the transition moment between $2.0 < R < 2.6\ a_0$. The transition moments of other higher lying states of $^2\Pi$ and $^2\Sigma^+$ symmetry are also significantly affected by Rydberg behavior.

For the (3) $^2\Pi$ state, we conducted test calculations in which the natural orbitals of the (3) $^2\Pi$ state were iterated

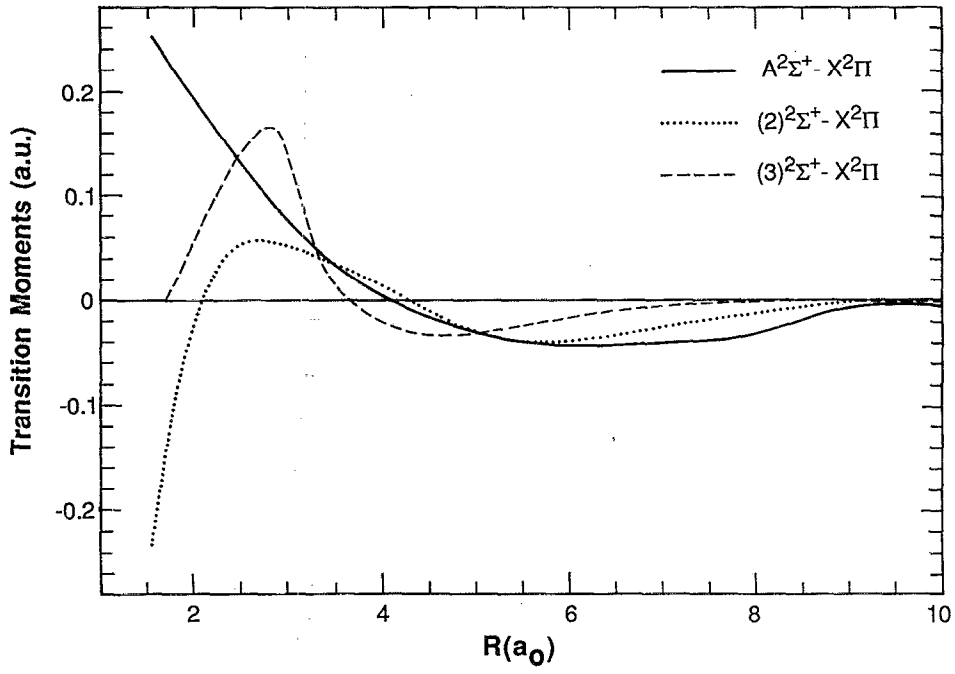

FIG. 5. Transition dipole moments between X state and states of $^2\Sigma^+$ symmetry.

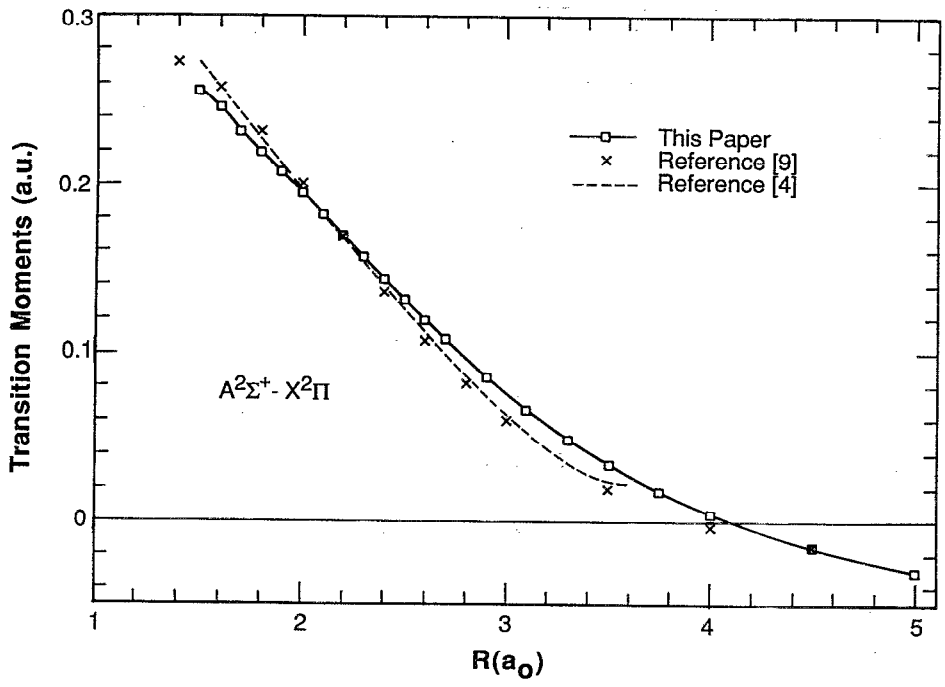

FIG. 6. Comparison of A–X transition dipole moments.

twice and then the transition moment with the $X\,^2\Pi$ state was computed. The results showed that the transition moment varied no more than 9% from the values listed in Table IX.

C. Radiative lifetimes of $A\,^2\Sigma^+$ vibrational levels

The probability of a spontaneous transition from the vibrational level v' of an upper electronic state to the vibrational level v'' of a lower electronic state with no change in electronic spin is given by

$$A_{v'v''} = 2.026\times 10^{-6} g \nu^3_{v'v''} |D_{v'v''}|^2 s^{-1}, \tag{7}$$

where g is a statistical weighting factor equal to 2 for Σ–Π transitions and 1 for all other transitions, $\nu_{v'v''}$ is the transition frequency in cm^{-1} and

$$D_{v'v''} = \langle \chi_{v'}(R)|D(R)|\chi_{v''}(R)\rangle \tag{8}$$

is the vibrationally averaged transition dipole moment in atomic units.

For the case of $A\,^2\Sigma^+$–$X\,^2\Pi$, spontaneous transitions into the vibrational continuum of the $X\,^2\Pi$ state cannot occur for vibrational levels $v' < 6$ of the $A\,^2\Sigma^+$ state. Therefore the lifetime τ for $v' < 6$ is given by

$$\tau_{v'} = 1/\Sigma_{v''} A_{v'v''}. \tag{9}$$

The absorption oscillator strength from the v'' level of the X state to the v' level of the A state is given by

$$f_{v''v'} = \tfrac{2}{3}\Delta E_{v'v''} |D_{v'v''}|^2. \tag{10}$$

Table X lists values for $f_{v''v'}$, $A_{v'v''}$, and $\tau_{v'}$. Our lifetime values are compared to other theoretical and experimental results.

The vibrational wave functions $\chi_v(R)$ were obtained by numerical integration of the radial Schrodinger equation (5). For the potential curve of the $A\,^2\Sigma^+$ state we used the RKR curve provided by Sheasley and Mathews[2] supplemented in the repulsive portion by our calculated points which were interpolated and smoothly attached at $R = 2.20\ a_0$. Between $R = 4.42\ a_0$ and $R = 5.87\ a_0$, the curve was extended beyond the last point provided by Sheasley and Mathews[2] by setting $\rho = R - R_e$ and using

$$V(\rho) = -D_e[1 + 1.51(\rho)]e^{-1.51\rho},$$

which connects the RKR curve smoothly to the correct asymptotic form as given by Eq. (2). For D_e, we used 1.856 eV (Hotop *et al.*[16]). In order to check the accuracy of our potential curves for the A and X states, we calculated Franck–Condon factors ($|\langle \chi_{v'}|\chi_{v''}\rangle|^2$) and R centroids (R_c) for the A–X transition for all (v',v'') band progressions considered in this study:

$$R_c = \frac{\langle \chi_{v'}|R\,|\chi_{v''}\rangle}{\langle \chi_{v'}|\chi_{v''}\rangle}.$$

These were compared to previous results,[2,5,6] and good agreement was found in all cases (at least three significant figures).

We used a value of $J = 1/2$ and $\Omega = 1/2$ for the $A\,^2\Sigma^+$ state and $J = 3/2$, $\Omega = 3/2$ for the $X\,^2\Pi$ state in the centrifugal distortion term of Eq. (5) and for the spin–orbit energy in the $^2\Pi_{3/2}$ state we used $A = -643.7\ \mathrm{cm}^{-1}$.[2] For the $A\,^2\Sigma^+$ ($v' = 0$) level we obtained a lifetime of $\tau_0 = 1.73\ \mu$s. Repeating the calculation with a value of $J = 9/2$ in the A state and $J = 11/2$ in the X state we obtained a value for τ_0 of 1.76 μs. Werner *et al.*[10] obtain a value of 2.51 μs using their MCSCF-SCEP dipole moment and Martner *et al.*[4] from their experimental results inferred an average value of $3.4 \pm 0.4\ \mu$s for the lifetime of five rovibrational levels in the $\Omega = 3/2$ subband of the A–X transition.

TABLE X. Absorption oscillator strengths $f_{v''v'}$, radiative transition probabilities $A_{v'v''}$, and radiative lifetimes for the A–X transition.

$f_{v''v'}$ ($\times 10^{-4}$)

v'' \ v'	0	1	2	3	4	5	6
0	2.937	4.150	3.580	2.406	1.415	0.772	0.404
1	2.359	0.177	0.514	1.910	2.560	2.362	1.803
2	0.762	0.589	1.028	0.136	0.181	1.007	1.685
3	0.117	0.741	0.000	0.613	0.665	0.126	0.049
4	0.008	0.224	0.334	0.195	0.073	0.511	0.485
5	0.000	0.025	0.223	0.055	0.296	0.031	0.113
6	0.000	0.001	0.036	0.144	0.002	0.171	0.161
7	0.000	0.000	0.001	0.035	0.060	0.043	0.034
8	0.000	0.000	0.000	0.001	0.024	0.012	0.061

$A_{v'v''}$ (10^5 s^{-1})

v' \ v''	0	1	2	3	4	5	6
0	3.096	2.053	0.542	0.067	0.004	0.000	0.000
1	4.875	0.173	0.477	0.490	0.119	0.010	0.000
2	4.627	0.559	0.934	0.000	0.205	0.110	0.014
3	3.391	2.283	0.137	0.515	0.136	0.031	0.067
4	2.159	3.334	0.200	0.619	0.057	0.191	0.001
5	1.264	3.324	1.210	0.128	0.439	0.022	0.102
6	0.707	2.721	2.184	0.054	0.456	0.089	0.107

$\tau_{v'}$ (μs)

v'	This work	Ref. 10 (MCSCF-SCEP)	Ref. 3 (expt.)	Ref. 4 (expt.)	Ref. 6 (expt.)
0	1.74	2.51	2.58	3.40 ± 0.4	3.40[a]
1	1.63	2.12	2.30		2.87
2	1.55	1.91	2.22		2.60
3	1.52	1.78	2.06		2.44
4	1.52	1.71	1.94		2.36
5	1.53	1.69	1.90		2.34
6	1.57	1.68	1.85		2.33

[a]Normalized to τ_0 of Ref. 4.

Both our results (Table X) for the A–X dipole moment and the MCSCF-SCEP results of Werner *et al.*[10] show that slightly over 50% of the total transition probability from the $A\,^2\Sigma^+$ ($v'=0$) level is due to the ($v'=0, v''=0$) transition. Therefore a lifetime of $\tau_0 = 3.4$ μs should give a value of 1.50×10^{-4} for the (0,0) oscillator strength. The value of $f_{00} = 1.08 \pm 0.13\times10^{-4}$ stated by Martner *et al.*[4] is inconsistent with these results for A–X transition probabilities and is considerably smaller than our value of 2.94×10^{-4} and the value 2.11×10^{-4} of Werner *et al.*[10]

We stated in the previous section that our calculated value for the A–X transition moment could vary in the Franck–Condon region by as much as 0.011 a.u. with respect to different orbital sets. A decrease in our calculated dipole moment for the A–X transition by this amount would result in a lifetime of $\tau_0 = 2.25$ μs and an oscillator strength of $f_{00} = 2.38\times10^{-4}$. Werner *et al.*[10] acknowledge a probable uncertainty for the radiative lifetime of 25% due to a 0.01 a.u. variation between their PNO-CI and MCSCF-SCEP calculations of the dipole moment. Therefore the results of Werner *et al.*[10] and this work for the lifetimes and oscillator strengths of A–X transitions are consistent within the probable errors of each calculation.

The Franck–Condon factor for the $v'=2 \rightarrow v''=3$ transition is less than 4×10^{-4} and the A_{23} transition probability is a factor of more than 10^6 smaller than the A_{00} transition probability. The absence of the (2,3) band in the emission spectra obtained by Glenewinkel-Meyer *et al.*[5] and Rodriguez *et al.*[6] is the result of the unusually small A_{23} transition probability.

The behavior of our lifetimes $\tau_{v'}$ as v' increases differs from that of the other studies listed in Table X[3,6,10] with the variation of our calculated lifetimes from $v'=0$ to $v'=6$ being considerably less. Our calculated lifetimes decrease from $v'=0$ up to $v'=4$ ($\tau_4/\tau_0 = 0.87$) and then begin to increase for $v'=5$ and 6 ($\tau_6/\tau_0 = 0.90$). The smaller range of variation of our lifetimes compared to the other studies listed in Table X is due to the more moderate slope of our A–X dipole moment while the larger value of our dipole moment between $2.4 < R < 4.0\,a_0$ causes significant A–X transition strength to be deposited over a range of higher lying v'' levels which have smaller $\nu^3_{v'v''}$ factors and consequently longer lifetimes than in previous studies.[3,6,10]

In Fig. 3, we see that the $A\,^2\Sigma^+$ state is crossed by the $^4\Pi$, $^2\Sigma^-$, and $^4\Sigma^-$ states between 4.61 and 4.68 a_0 with the $^4\Pi$ state crossing at 4.65 a_0 only 280 cm^{-1} below the $v'=7$

vibrational level. Predissociation of the A state vibrational levels by spin–orbit coupling would be dominated by the $^4\Pi$ state since its principal configuration $(\cdots 5\sigma 6\sigma 2\pi^3)$ differs by only one spin orbital from that of the A state $(\cdots 5\sigma 2\pi^4)$. Predissociation of the $v'=7$ level of the A state is likely since it has not been observed in previous studies[2,5,6] and since it would have significant transition probability if it were able to radiate to the $v''=1$ and 2 levels of the X state ($A_{71}=2.0\times10^5\ s^{-1}$ and $A_{72}=2.6\times10^5\ s^{-1}$). Raferty and Richards[9] in a single configuration approximation for the $A\ ^2\Sigma^+$ and $^4\Pi$ states calculated a spin–orbit matrix element $\langle A\ ^2\Sigma^+|H_{so}|^4\Pi_{1/2}\rangle = 260\ cm^{-1}$. For the $v'=7$ level the transition probability is estimated to be

$$\Gamma = 3.65\times10^{11}|\langle\chi_{v'}|\chi_k\rangle|^2 s^{-1},$$

where χ_k is the energy normalized continuum wave function for the $^4\Pi$ state at the energy of the bound level. We obtain a value of 2.1×10^{-2} a.u. for the bound–continuum overlap resulting in a predissociation probability of $1.6\times10^8\ s^{-1}$ which shows that the levels $v'\geqslant 7$ are indeed predissociated.

D. Dipole moments for the $X\ ^2\Pi$ and $A\ ^2\Sigma^+$ states

The dipole moments as a function of R for the $X\ ^2\Pi$ and $A\ ^2\Sigma^+$ states are given in Table XI. Referred to the center of mass of the molecule, our results for the $X\ ^2\Pi$ state may be represented by the following expansion valid in the range $1.0<R<1.9$ Å (μ in D, R in Å):

$$\mu(R) = 1.70 + 2.38(R-R_e) + 0.946(R-R_e)^2 - 0.518(R-R_e)^3.$$

They are in good agreement with the result of Werner *et al.*:[10]

$$\mu(R) = 1.642 + 2.370(R-R_e) + 1.020(R-R_e)^2 - 0.604(R-R_e)^3.$$

We tested the stability of our results for the dipole moment function with respect to different orbital sets. A natural orbital iteration was performed at R_e in which the natural orbitals of the $X\ ^2\Pi$ state which were output in the previous calculation were used as initial input orbitals in the the next calculation. After two successive cycles of iteration the dipole moment, results were found to vary not more than 3% from the results obtained from the initial orbital set.

A fit of the results for the dipole moment function of the $A\ ^2\Sigma^+$ state valid in the range $1.3<R<2.0$ Å gave

$$\mu(R) = 2.91 + 3.84(R-R_e) + 0.684(R-R_e)^2 - 0.488(R-R_e)^3,$$

where R_e is now the nuclear separation at the potential well minimum of the $A\ ^2\Sigma^+$ state. The stability of the dipole moment function of the $A\ ^2\Sigma^+$ state was found to be comparable to that of the $X\ ^2\Pi$ state.

Using vibrational wave functions obtained by solving Eq. (5), we computed the lifetime of the $X\ ^2\Pi(v=1\rightarrow0)$ rotationless transition which is given in Table XII along with other theoretical and experimental results. Our result for HCl^+ lies within the error limits of the measured lifetimes. The results of Heninger *et al.*[7] for both HCl^+ and DCl^+ are significantly smaller than all other determinations. The ratio of the lifetimes of the two isotopes DCl^+ and HCl^+ (τ_D/τ_H) is also listed for each study. Our result $\tau_D/\tau_H = 3.70$ equals the ratio $(\omega_H/\omega_D)^4$ (Table VIII) expected for harmonic wave functions in these lowest vibrational bands. The data of Sheasley and Mathews[2] give $(\omega_H/\omega_D)^4 = 3.77$. Also listed in Table XII are transition probabilities for other vibrational levels up to $v=9$ of the $X\ ^2\Pi$ state.

TABLE XI. Dipole moments (Debye) of $X\ ^2\Pi$ and $A\ ^2\Sigma^+$ states.

R (a_0)	R (Å)	$X\ ^2\Pi$	$A\ ^2\Sigma^+$
1.80	0.95	0.98	0.61
1.90	1.01	1.06	0.83
2.00	1.06	1.16	1.05
2.10	1.11	1.25	1.27
2.20	1.16	1.36	1.49
2.30	1.22	1.47	1.71
2.40	1.27	1.59	1.92
2.50	1.32	1.71	2.14
2.60	1.38	1.84	2.35
2.70	1.43	1.98	2.56
2.90	1.53	2.26	2.97
3.10	1.64	2.55	3.37
3.30	1.75	2.86	3.75
3.50	1.85	3.17	4.10
3.75	1.98	3.56	4.50

E. Photodissociation of HCl^+

Absorption of radiation from the $X\ ^2\Pi$ state of HCl^+ into the repulsive states of $^2\Sigma^+$, $^2\Sigma^-$, $^2\Pi$, and $^2\Delta$ symmetries causes dissociation of the molecule. Our calculations of the fourth states of $^2\Sigma^+$ and $^2\Pi$ symmetry indicate that they do not play a significant role in interstellar photodissociation due their large excitation energies and small transition dipole moments with the X state. Only absorption into the (2) $^2\Pi$ state results in protons plus neutral chlorine, while absorption into all other repulsive states considered produces Cl^+ and neutral hydrogen (Figs. 2 and 3).

The photodissociation cross sections for transitions out of the $X\ ^2\Pi$ state as functions of energy absorbed E are

$$\sigma_v(E) = 2\pi^2\alpha\left.\frac{df}{dE}\right|_{vk}, \tag{11}$$

where α is the fine structure constant and $df/dE|_{vk}$ is the bound–continuum differential band oscillator strength:

$$\left.\frac{df}{dE}\right|_{vk} = \frac{2}{3}\Delta E_{vk}|D_{vk}|^2 \tag{12}$$

with ΔE_{vk} being the transition energy in a.u., and the bound–continuum matrix element D_{vk} given by

$$D_{vk} = \langle\chi_v(R)|D(R)|\chi_k(R)\rangle, \tag{13}$$

also in a.u.

The energy normalized continuum wave function is obtained by numerical integration of

TABLE XII. Transition probabilities for spontaneous emission (s^{-1}) for the $X^2\Pi$ state of HCl^+ and the radiative lifetime of the $X^2\Pi(v=1)$ level (ms).

v	Transition probabilities A_v^{v+1}	A_v^{v+2}	A_v^{v+3}
0	205.6	6.637	0.1188
1	382.4	20.43	0.5241
2	530.4	41.89	1.416
3	648.5	71.40	3.167
4	736.9	108.8	6.161
5	796.3	153.4	10.99
6	827.9	204.3	18.25
7	834.0	259.9	28.52
8	816.7	318.2	...
9	778.9	...	...

	$X^2\Pi(v=1\rightarrow0)$ Radiative lifetime			
	Experimental Ref. 7	Ref. 8	Theoretical Ref. 10	This work
$HCl^+(v=1\rightarrow0)$	3.4 ± 1.2	4.5 ± 1	4.61	4.86
$DCl^+(v=1\rightarrow0)$	13.2 ± 3	17 ± 4	19.3	18.0
τ_D/τ_H	3.88	3.8	4.19	3.70

$$-\frac{\hbar^2}{2\mu}\frac{d^2}{dR^2}\chi_k(R) + \left\{V(R)+\frac{[J(J+1)]}{2\mu R^2}-\frac{\hbar^2k^2}{2\mu}\right\}\chi_k(R)=0 \qquad (14)$$

with k being the wave number of asymptotic relative nuclear motion. The continuum wave function $\chi_k(R)$ was taken to have the asymptotic form

$$\chi_k(R)\sim\left(\frac{2\mu}{\pi\hbar^2k}\right)^{1/2}\sin\left(kR-\frac{J\pi}{2}+\delta_J\right),$$

where δ_J is the elastic scattering phase shift. A Boltzmann average over the initial rotational states showed that the photodissociation cross sections are insensitive to the rotational population in the the $v=0$ $X^2\Pi$ level and changed by less than 2% near their peak and by 15% at energies at which the cross sections are 2 orders of magnitude less.

Photodissociation cross sections, neglecting rotation, from the $v=0$ level of the X state to dipole accessible states are shown in Figs. 7 and 8. Only the $v=0$ level would be significantly populated in most atmospheric and interstellar environments.

The similarity in the shape and magnitude of the photodissociation cross sections for the $^2\Sigma^-$ and $^2\Delta$ states is due to

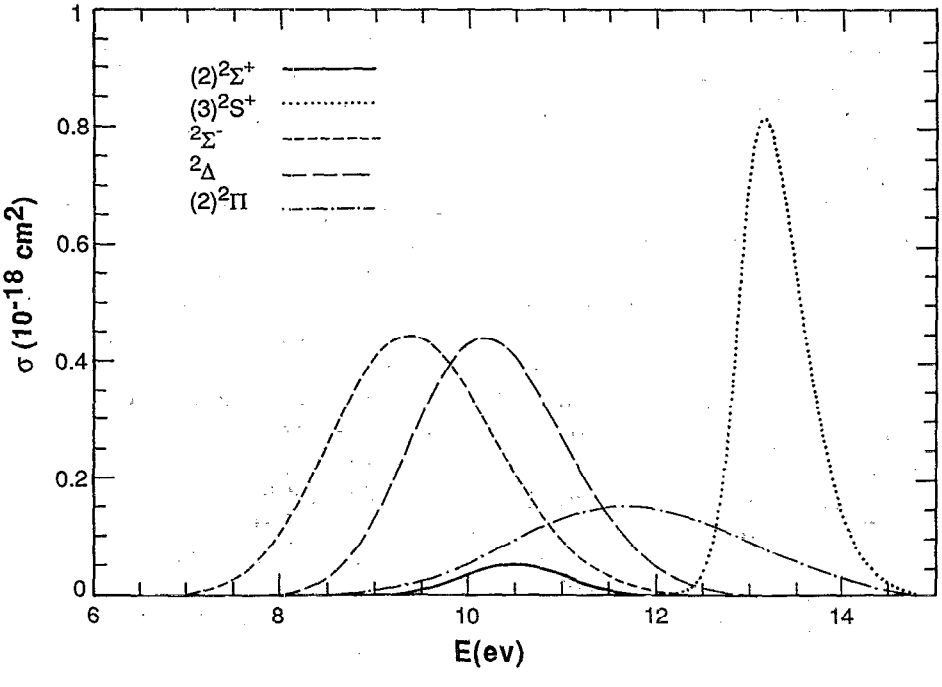

FIG. 7. Photodissociation cross sections from X state.

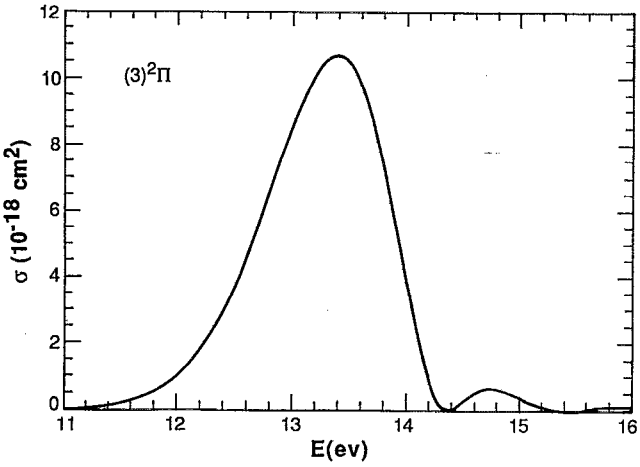

FIG. 8. Photodissociation cross section from X state into (3) $^2\Pi$ state.

their similar transition moments (Fig. 4) with the $X\,^2\Pi$ state. The asymmetric shape of the X–(3) $^2\Pi$ photodissociation cross section is due to the rapid rise in the transition moment in the neighborhood of R_e of the ground state and the irregular behavior of the transition moment at small nuclear separations ($R < 2.2\ a_0$) due to avoided crossings. The 9% uncertainty in our calculation for the X–(3) $^2\Pi$ transition moment (Sec. III B) implies that this calculated photodissociation cross section is accurate to within 20%.

In the wavelength region 112–155 nm, photodissociation of HCl^+ will proceed through the $^2\Sigma^-$ and $^2\Delta$ states leading to the production of $Cl^+(^3P)$ and metastable $Cl^+(^1D)$. Between 100–110 nm, photodissociation through the (2) $^2\Pi$ state dominates and produces $Cl^+(^3P)$ though the peak cross section for this process is three times less than the peak cross sections of the $^2\Sigma^-$ and $^2\Delta$ states.

For wavelengths shortward of 100 nm the cross section for photodissociation through the (3) $^2\Sigma^+$ state shows that significant production of metastable $Cl^+(^1S)$ is possible. The photodissociation of HCl^+ in this wavelength region is dominated, however, by the (3) $^2\Pi$ state which for $\lambda < 95$ nm has a cross section that is more than an order of magnitude greater than any other presented here and demonstrates that production of metastable $Cl^+(^1D)$ is the major end product of photodissociation of HCl^+ at ultraviolet wavelengths.

IV. SUMMARY

We have computed potential curves for the ten lowest lying states of HCl^+ giving a balanced description of Rydberg–valence mixing for repulsive states that are important in photodissociation. Calculations have also been made of the dipole moment functions of the $X\,^2\Pi$ and $A\,^2\Sigma^+$ states and transition moment functions from the X state to dipole-allowed excited states.

Our computed values for the A–X dipole moment are larger than those from previous determinations[5,6,10] for $R > 2.4\ a_0$. For the $A\,^2\Sigma^+$ state, our results for the radiative lifetimes are consistent within probable errors with previous theoretical results[10] but are a factor of two less than experimental determinations.[4,6] Vibrational levels $v' \geqslant 7$ of the $A\,^2\Sigma^+$ state are predissociated primarily by spin orbit coupling to the $^4\Pi$ state.

Our radiative rate (Table XII) for the $X\,^2\Pi(v = 1 \rightarrow 0)$ transition is in good agreement with experimental results.[7,8]

The major pathway to photodissociation of HCl^+ in the wavelength region $\lambda < 100$ nm is through the (3) $^2\Pi$ state leading to the production of metastable $Cl(^1D)$.

ACKNOWLEDGMENTS

The authors are pleased to thank Dr. Evelyn M. Goldfield, Dr. Roberta P. Saxon, and Dr. M. Yoshimine for helpful discussions. This research was conducted using the Cornell National Supercomputer Facility, a resource of the Center for Theory and Simulation in Science and Engineering at Cornell University, which is funded in part by the National Science Foundation, New York State, and the IBM Corporation and members of the Corporate Research Institute. The work of A. Dalgarno was supported in part by the U.S. Department of Energy, Division of Chemical Sciences, Office of Energy Research. The work of Atul D. Pradhan was supported by the National Science Foundation through its funding of the Institute for Theoretical Atomic and Molecular Physics.

APPENDIX

In order to test the accuracy of our numerical computations, we employ the sum rule of Stephens and Dalgarno.[18]

If $\{\chi_v, \chi_k\}$ is a complete set of discrete, bound vibrational wave functions χ_v and energy normalized continuum wave functions χ_k, and D is an operator connecting these states to the vibrational level of another electronic state ψ, then, in general,

$$\langle \psi | D^2 | \psi \rangle = \sum_v |\langle \chi_v | D | \psi \rangle|^2 + \int_\epsilon |\langle \chi_{k(\epsilon)} | D | \psi \rangle|^2 \, d\epsilon, \tag{15}$$

where the wave number and energy of relative motion are related by $\epsilon = \hbar^2 k^2 / 2\mu$.

For radiative decay from the $A\,^2\Sigma^+(v' = 0)$ level, we included in the sum all levels ($v'' \leqslant 15$) of the $X\,^2\Pi$ state which lie below the $A\,^2\Sigma^+(v' = 0)$ level. Only the sum over discrete vibrational levels is relevant and the sum rule was satisfied to within 0.0023%. The higher levels of the $A\,^2\Sigma^+$ state similarly satisfied the sum rule to within 0.001%.

For transitions from the X state to continuum states, only the second term on the right-hand side contributes. For the $X\,^2\Pi$–$^2\Delta$ transition, the inclusion in the integral of an energy range of ± 3 eV around the peak of the oscillator strength (10.2 eV) satisfies the sum rule to within one part in 5.9×10^3. In all other such cases, the sum rule was similarly satisfied to better than 0.02%.

[1] E. F. van Dishoeck, M. C. van Hemert, and A. Dalgarno, J. Chem. Phys. **77**, 3693 (1982).
[2] W. D. Sheasley and C. W. Mathews, J. Mol. Spectrosc. **47**, 420 (1973).
[3] G. R. Mohlman, K. K. Bhutani, and F. J. de Heer, Chem. Phys. **21**, 127 (1977).
[4] C. C. Martner, J. Pfaff, N. H. Rosenbaum, A. O'Keefe, and R. J. Saykally, J. Chem. Phys. **78**, 7073 (1983).
[5] T. Glenewinkel-Meyer, B. Muller, C. Ottinger, and H. Tischer, J. Chem. Phys. **88**, 3475 (1988).
[6] A. Rodriguez, and J. Campos, J. Chem. Phys. **86**, 4401 (1987).
[7] M. Heninger, S. Feinstein, G. Mauclaire, R. Marx, and Y. M. Yang, J. Chem. Soc. Faraday Trans. 2 **85**, 1705 (1989).
[8] G. Javahery, J. Glosik, M. Tichy, N. D. Twiddy, and E. E. Ferguson, Int. J. Mass Spectrom. Ion Proc. **97**, 203 (1990).
[9] J. Raferty and W. G. Richards, J. Phys. B **6**, 1301 (1973).
[10] H. J. Werner, P. Rosmus, W. Schatzl, and W. Meyer, J. Chem. Phys. **80**, 833 (1984).
[11] A. D. McLean (private communication).
[12] R. P. Saxon and B. Liu, J. Chem. Phys. **85**, 2099, (1986).
[13] R. P. Saxon, K. Kirby, and B. Liu, J. Chem. Phys. **73**, 1873 (1980).
[14] E. Reinsch, W. Meyer, Phys. Rev. A **14**, 915 (1976).
[15] C. F. Fischer, Atomic and Nuclear Data Tables **12**, 88 (1973).
[16] H. Hotop, G. Hubler, and L. Kaufhold, Int. J. Mass Spectrom. Ion Phys. **17**, 163 (1975).
[17] P. Natalis, P. Pennetreau, L. Longton, and J. E. Collin, J. Electron Spectrosc. Relat. Phenom. **27**, 267 (1982).
[18] T. L. Stephens and A. Dalgarno, J. Quantum. Spectrosc. Radiat. Transfer **12**, 569 (1972).